ACS APPLIED MATERIALS & INTERFACES

Research Article

www.acsami.org

Band Gap Engineering of In_2TiO_5 for H_2 Production under Near-infrared Light

Ding Wei, Lihua Yao, Song Yang, Zhentao Cui, Bingxue Wei, Minhua Cao,* and Changwen Hu*

Key Laboratory of Cluster Science, Ministry of Education of China, Beijing Key Laboratory of Photoelectronic/Electrophotonic Conversion Materials, Department of Chemistry, Beijing Institute of Technology, Beijing 100081, People's Republic of China

Supporting Information

ABSTRACT: In_2TiO_5, containing both early transition metal (d^0) and p-block metal (d^{10}), is a very promising candidate for possible application in H_2 production because of its suitable edges of conduction and valence bands and the crystal structure, which is considered to favor mobility of charge carriers. Herein we report, for the first time, the synthesis of novel oxygen vacancies (OV), N-doped In_2TiO_5 (OV,N–In_2TiO_5) with controllable band gap. The resultant OV,N–In_2TiO_5 sample was prepared by a multistep sol–gel calcination process and studied as a near-infrared (NIR) light-driven photocatalyst for H_2 production. OV and N-doping can effectively extend the photoresponse of In_2TiO_5 to the NIR region due to an interband springboard and the reduced band gap, thus leading to efficient NIR light photocatalytic H_2 production activity with Pt as a cocatalyst.

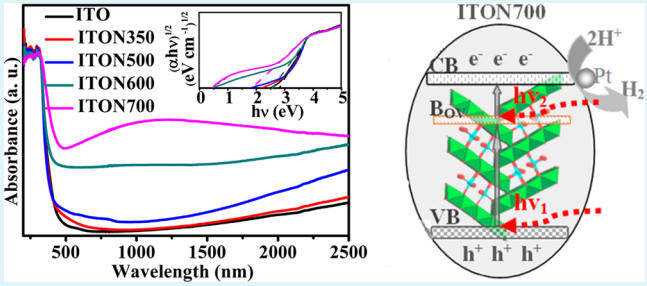

KEYWORDS: *In_2TiO_5, oxygen vacancies, nitrogen doping, near-infrared light, photocatalysis*

1. INTRODUCTION

Over the past years, intense research efforts have been devoted to direct conversion of solar energy to chemical energy by photocatalysis processes, because it is clean and renewable.[1−4] This has led to amazing developments of various semiconductor photocatalytic materials, especially ultraviolet (UV) and visible (Vis) light-responsive photocatalysts that can efficiently utilize the abundant solar energy.[5−8] It is well-known that visible light accounts for nearly 50% of solar light energy, while the residual 7% and 43% are made up of UV light and infrared (IR) light, respectively. Thus, compared to the great amount of work done in the UV and Vis light range, IR light, which constitutes almost half the solar energy, has been overlooked and rarely used. To the best of our knowledge, only a very limited number of materials with IR light-driven photocatalytic activity have been developed to date, such as carbon-doped TiO_2, $NaYF_4$:Yb, Tm/CdS, $Cu_2(OH)PO_4$,Bi_2WO_6, black TiO_2, dye-sensitized g-C_3N_4, etc.[9−14] Among the studied IR light photocatalysts, most are upconversion materials, which possess a very narrow absorption band and cannot use sunlight efficiently. Very recently, it is interesting to note that there are a few reports on H_2 production by photocatalytic processes under near-infrared (NIR) light irradiation. For example, Yang and co-workers[15] broke through the restriction of standard reaction mechanism of water splitting and proposed a new photosynthesis mechanism for producing H_2 in which NIR light can be used. The new reaction model was verified in surface-functionalized hexagonal boron–nitride bilayers by electronic and optical calculations. Tachikawa and co-workers[16] reported that Pt-tipped Au nanorods show strong absorption at 700–1200 nm and exhibit efficient photocatalytic H_2 evolution under Vis–NIR light. Li and co-workers[17] used a highly asymmetric zinc phthalocyanine derivative (Zn-*tri*-PcNc) as the sensitizer of g-C_3N_4 for extremely efficient NIR light-driven photocatalytic H_2 production. The sensitizer Zn-*tri*-PcNc can remarkably extend the spectral response region of g-C_3N_4 from ∼450 nm to more than 800 nm. Although none of them focused on wavelengths longer than 760 nm, these studies present a promising future for NIR light-driven photocatalysis, and therefore, developing new NIR light responsive photocatalysts is highly desirable for further investigation of photocatalysis.

In order to extend the spectral response of wide band gap oxide semiconductors toward the long-wavelength region, many attempts have been made, such as photosensitizing, doping, and heterogenization.[18−20] It has been addressed that, for Vis and NIR light-induced photocatalytic utilization, nitrogen doping is proposed to be an effective and especially active means since the study of Asahi et al.[21−24] Besides nitrogen doping, oxygen vacancies (OV) have been widely used for narrowing optical band gap, and some recent reports mainly focus on TiO_2, ZnO, In_2O_3, BiOCl, and so on.[25−28] These studies show that the OV can induce a new in-gap band that can increase Vis light absorption, leading to enhanced photocatalytic activity. Compared to conventional cation doping, OV as self-doping, without introduction of any

Received: June 26, 2015
Accepted: August 31, 2015
Published: August 31, 2015

DOI: 10.1021/acsami.5b05706
ACS Appl. Mater. Interfaces 2015, 7, 20761–20768

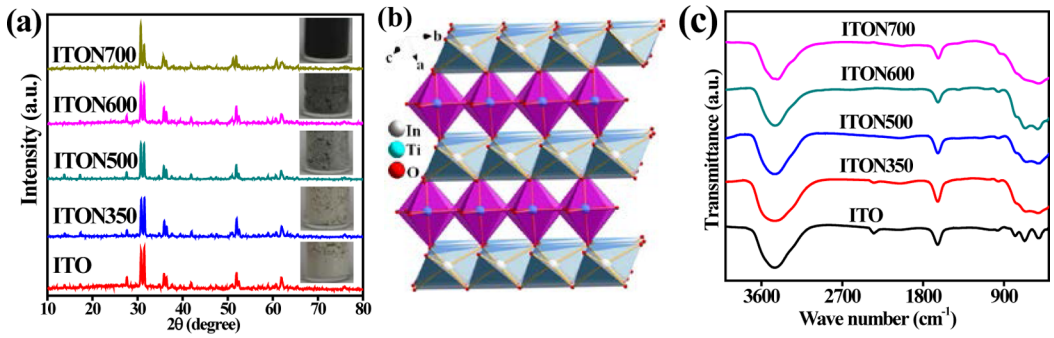

Figure 1. (a) X-ray diffraction (XRD) patterns and photographs of as-prepared ITO samples. (b) Schematic illustration of In_2TiO_5 crystal structure. (c) FT-IR patterns of as-synthesized samples.

impurity elements, is more favorable for preserving the intrinsic crystal structure of semiconductors.

The physicochemical properties of titanate- and indium-based mixed oxide semiconductors, such as $SrTiO_3$, $BaTiO_3$, $CaTiO_3$, $In_{1-x}Ni_xTaO_4$, $CaIn_2O_4$, and In_2TiO_5, have been investigated in great detail because of both fundamental scientific knowledge and their widespread technological applications in various fields. Some of them display good photocatalytic activity and chemical stability.[29−33] Recently, the ternary In_2TiO_5 (abbreviated as ITO) has been extensively studied as a new class of photocatalyst, which was reported to show excellent activity for water splitting or dye degradation.[34−36] In_2TiO_5 contains both early transition metal (d^0) and p-block metal (d^{10}) that fulfill desirable criteria required for active photocatalysts. It possesses a three-dimensional tunneling structure, which is built by octahedral [TiO_6] and [InO_6] motifs (Figure 1b). It has been addressed that the [InO_6] octahedron in the crystal structure is beneficial for mobility of charge carriers, thus improving the photocatalytic activity.[32] Unfortunately, due to the larger energy band gap of ITO, almost all reported works focus on its UV and Vis light-driven photocatalysis. So far, there are no investigations concerning its NIR light-induced photocatalysis.

Herein, we use a facile strategy, OV and nitrogen doping engineering, to accomplish NIR light-induced photocatalysis of ITO for H_2 production from water. The OV, N-doped In_2TiO_5 (OV,N−In_2TiO_5) sample was prepared by annealing pristine In_2TiO_5 in NH_3 atmosphere at 600−700 °C for 2 h. OV and N-doping have evidently changed optical properties and energy band structure of ITO, which has been confirmed by UV−vis−NIR optical spectroscopy and density functional theory (DFT) calculations. The photocatalytic performance of OV,N−In_2TiO_5 was evaluated by measuring photocurrent response and photocatalytic H_2 production under NIR light irradiation. To the best of our knowledge, this represents the first case of realizing NIR photocatalysis of In_2TiO_5 for H_2 evolution with Pt as a cocatalyst.

2. EXPERIMENTAL SECTION

Chemicals and Reactants. Indium chloride ($InCl_3$, 99.9% metals basis) was purchased from Aladdin (Shanghai) Chemistry Co., Ltd. Nitric acid (HNO_3, AR), tetrabutyltitanate [$Ti(C_4H_9O)_4$, AR], and ethylenediaminetetraacetic acid disodium salt ($C_{10}H_{14}N_2Na_2O_8{\cdot}2H_2O$, denoted as ED2Na, AR) were purchased from Wei Si Chemical Co. (Beijing). All chemical reagents were of analytical grade and used without further purification.

Synthesis of Pristine In_2TiO_5. $InCl_3$ (0.4 mmol) and $Ti(C_4H_9O)_4$ (0.2 mmol) were added to a nitric acid aqueous solution (10 mL, 1 mol·L^{-1}), which was stirred to form a transparent solution. ED2Na (0.66 mmol) was dissolved in distilled water (10 mL) to form a ED2Na solution, which then was added into above mixed salt solution drop by drop. After the solution was stirred for 30 min, the pH value of the mixed solution was adjusted to 5. The solution was then heated at 70 °C in oil bath for ∼30 h until a gel was obtained. The resultant gel was transferred into a combustion boat and calcined at 250 °C for 10 h in a tubular furnace. After cooling, the product was collected and calcined for the second time at 950 °C for 2 h. Pristine In_2TiO_5 was finally obtained after the tube furnace was cooled to room temperature naturally; this product was denoted as ITO.

Synthesis of Pristine OV,N-In_2TiO_5. The resultant ITO powder was calcined at 350−900 °C for 2 h in NH_3 atmosphere to form different In_2TiO_5 samples. These as-obtained samples are denoted as ITON350, ITON500, ITON600, ITON700, ITON750, ITON800, and ITON900, respectively.

For comparison, another two In_2TiO_5 photocatalysts were prepared by annealing ITO powder at 600 and 700 °C in the tubular furnace for 2 h in H_2 atmosphere, which were named ITOH600 and ITOH700, respectively.

Characterization. Powder X-ray diffraction (PXRD) patterns of the samples were analyzed with monochromatized Cu Kα (λ = 1.541 78 Å) incident radiation by Bruker D8 Advance X-ray diffractometer operating at 40 kV voltage and 50 mA current. Fourier transform infrared (FT-IR) spectroscopy was recorded from KBr pellets in the range 400−4000 cm^{-1} on a Varian 3100 FT-IR spectrometer. The morphology and microstructure of the samples were observed by scanning electron microscopy (SEM, JEOL S-4800) and transmission electron microscopy (TEM, JEOL JEM-2010). X-ray photoelectron spectroscopy (XPS) was recorded with an Escalab 250 electron spectrometer to characterize the surface composition. CHN elemental analysis was conducted on ElementarVario Micro Cube. Electron paramagnetic resonance (EPR) was taken with an X-band EPR spectrometer (JEOL JES FA-200) operating at 9.065 GHz. UV−vis−NIR absorption spectra were measured on a Varian Cary 5000 UV−vis−NIR spectrophotometer. Spectra of the light from Xe lamp before and after filtration were detected on a wide-range optical spectrum analyzer Avaspec-NIR256 (Avantes). The calculations presented in this work were performed in the framework of density functional theory (DFT), as implemented in the Cambridge Sequential Total Energy Package (CASTEP) code. Time-based transient photocurrent response was performed on a CHI660D electrochemical workstation, where Pt electrode and saturated Ag/AgCl electrode were employed as counter and reference electrodes, respectively. A 300-W Xe lamp (CEL-HXF300, Jinyuan, λ = 760−1100 nm) was used as light source.

Theoretical Calculations. Electronic structures of pristine, N-, OV-, and OV,N-In_2TiO_5 were investigated within DFT as implemented in the CASTEP code, using exchange−correlation functional in the CA-PZ form of local density approximation (LDA). The electron−core interaction was represented via ultrasoft pseudopotentials with a plane-wave basis cutoff energy of 420 eV. The electronic exchange−correlation energy was treated within the framework of LDA. The self-consistent field (SCF) tolerance was all

DOI: 10.1021/acsami.5b05706
ACS Appl. Mater. Interfaces 2015, 7, 20761−20768

5×10^{-6} eV/atom. Fast Fourier transform (FFT) grids of basis in all models were 75 × 18 × 75. The κ-point sets of 1 × 6 × 1 were used for all models. The doped nitrogen and oxygen vacancies were located at a substitutional site for an O atom in the In_2TiO_5 crystal.

Photocatalytic H_2 Production by Near-infrared Light. NIR light photocatalytic H_2 production was performed with 0.04 g of photocatalyst suspended in 50 mL of methanol aqueous solution (25 vol %) in a closed circulation system by use of a xenon arc lamp (300 W, CEL-HXF300, Jinyuan) with a shutter window and a Vis-light cutoff filter (800 nm filter). $H_2PtCl_6 \cdot 6H_2O$ aqueous solution (1 mL, 1 mg of Pt·mL^{-1}) was dripped into the system to load Pt onto the surface of the photocatalyst by a photochemical reduction deposition method. The amount of H_2 was analyzed on a gas chromatograph (N2000, Zhejiang University) equipped with a thermal conductivity detector (N_2 carrier), which was connected to the gas circulating line. Detailed schematics of the equipment, optical spectrum analyzer, and emission spectrum of the light source are shown in Figures S2–S4 in Supporting Information.

3. RESULTS AND DISCUSSION

The typical preparation process for OV,N-In_2TiO_5 photocatalyst is based on a multistep sol–gel calcination method. Pristine ITO was first obtained by a sol–gel process, followed by a high-temperature treatment in air, which then was subjected to an ammonifying process in NH_3 at different temperatures. Clearly, with an increase in the NH_3-treated temperature (Figure 1a), the color of the samples gradually becomes dark gray, and this change may be partially due to bulk reduction of the ITO crystal by hydrogen from thermal decomposition of NH_3 at high temperature.[37] The crystal structure of the products before and after ammonification was characterized by X-ray diffraction (XRD) measurement. As shown in Figure 1a, for the sample before ammonification, all of the diffraction peaks can be indexed to a pure orthorhombic ITO phase (JCPDS ICDD 82-0326), which contains octahedral [TiO_6] and [InO_6] in a unit cell (Figure 1b).[38] If we changed the preparation conditions, such as complexing agent, pH value, and so on, impure ITO sample or unidentified mixtures would be formed (Figure S1). In addition, all the NH_3-treated samples still retained the orthorhombic ITO phase and no other byproducts, such as nitrogen-containing compounds, were detected from the XRD results. To further investigate the effect of ammonification temperature on the composition of samples, Fourier transform infrared (FT-IR) measurements were performed. It can be seen that no hydrocarbon peaks and amine complexes are observed (Figure 1c).[39]

As identified by scanning electron microscopy (SEM) in Figure 2a,b, the above as-synthesized ITO and ITON700 samples all consist of irregular rodlike submicrostructures and ammonification has almost no effect on the morphology and size of the samples. CHN elemental analysis (Table S1) proves the presence of 0.3 wt % N in ITON700 and 0.11 wt % N in ITON600. However, for ITON350 and ITON500, N contents are as low as 0.05 and 0.08 wt %, respectively, which are already beyond the detection limit of 0.1% for the instrument, indicating few N were incorporated into ITO matrix when the NH_3 treatment temperature was lower than 500 °C. The homogeneous distribution of N element on the surface of ITON700 was also confirmed by elemental mapping images (Figure 2b). Figure 2c,d show high-resolution transmission electron microscopy (HRTEM) images of ITO and ITON700, which are taken randomly from any areas. It can be seen that, for ITO, perfect lattice fringes without any defects are obtained, suggesting good crystallinity within the grains or at the grain

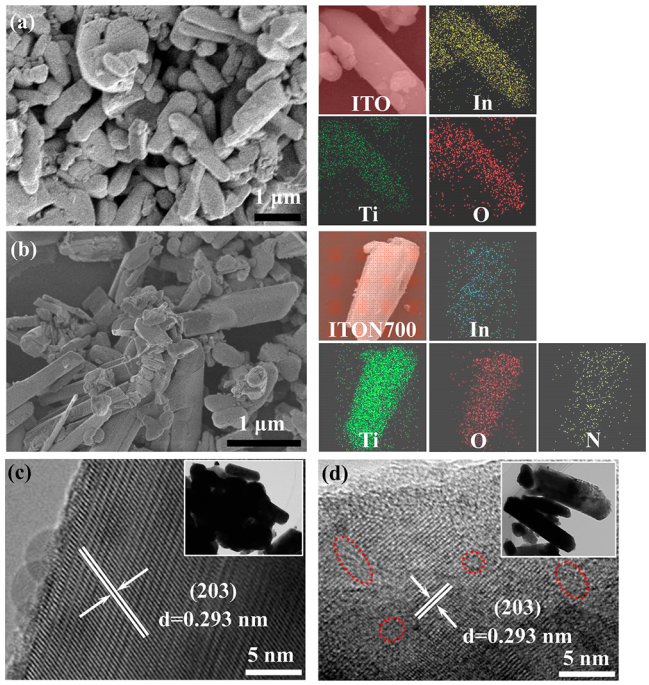

Figure 2. (a, b) SEM images of (a) ITO and (b) ITON700; on the right are elemental mapping images. (c, d) TEM and HRTEM images of (c) ITO and (d) ITON700. Red circles in panel d clearly show lattice defects and dislocations.

boundaries. However, some clear lattice defects and dislocations can be clearly observed in the well-defined crystalline structure of ITON700 (marked in red circles), demonstrating a novel defect-rich structure in the sample.[40]

Surface elemental components and valence states of the as-synthesized ITO samples were further determined by X-ray photoelectron spectroscopy (XPS) measurements, as shown in Figure 3. For ITON600 and ITON700 samples, the N 1s XPS spectra both exhibit four peaks at around 395.1, 396.3, 400.3, and 402.1 eV. The first two peaks can be attributed to TiN and O–In–N linkage, respectively, whereas the other two weak peaks are related to molecularly chemisorbed γ-N_2.[24,41,42] On the contrary, for ITO, ITON350, and ITON500, no evident

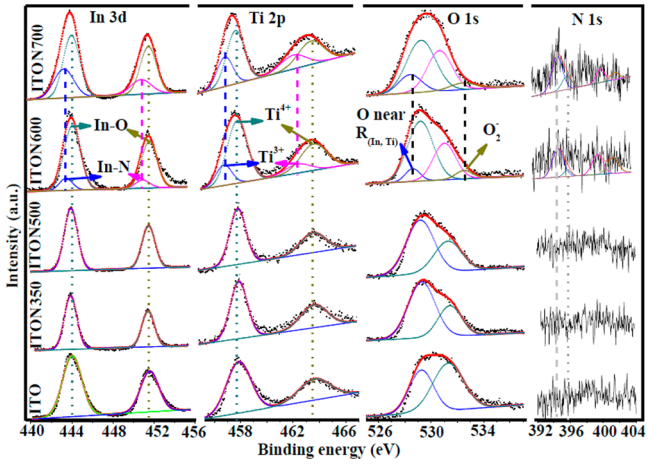

Figure 3. In 3d, Ti 2p, O 1s, and N 1s XPS spectra of ITO samples (top to bottom: ITON700, ITON600, ITON500, ITON350, and ITO).

DOI: 10.1021/acsami.5b05706
ACS Appl. Mater. Interfaces 2015, 7, 20761–20768

peaks were observed in N 1s XPS spectra, and their high-resolution In 3d XPS spectra (Figure 3) all show two peaks at binding energies of ~444.1 eV (In $3d_{5/2}$) and ~451.7 eV (In $3d_{3/2}$). However, for ITON600 and ITON700, the In 3d peaks can be deconvoluted into four peaks, which may originate from two components. The peaks centered at 444.3 and 451.8 eV can be ascribed to the In−O bond, while the other two peaks at lower binding energies (443.6 for In $3d_{5/2}$ and 451.1 eV for In $3d_{3/2}$) can be assigned to the In−N bond.[27,42] Furthermore, for ITON600 and ITON700, Gaussian fitting of the Ti 2p peak shows double peaks contributed from Ti^{3+} 2p and Ti^{4+} 2p. The peaks at 456.9 and 462.4 eV are characteristic of Ti^{3+}, while the peaks at 457.9 and 463.8 eV can be attributed toTi^{4+} $2p_{3/2}$ and Ti^{4+} $2p_{1/2}$, respectively.[43] Thus, it can be seen that after thermal treatment in NH_3 atmosphere at 600 and 700 °C, the Ti $2p_{3/2}$ and Ti $2p_{1/2}$ peaks shifted toward lower binding energies, which are mainly due to the introduction of oxygen vacancies into the In_2TiO_5 lattice. The presence of the oxygen vacancies in ITON600 and ITON700 was further confirmed by their corresponding O 1s XPS spectra (Figure 3). From the O 1s XPS spectra, we can see that the broad oxygen peak can be deconvoluted into four symmetric peaks centered at 529.0, 529.8, 531.1, and 532.7 eV. The highest binding energy at 532.7 eV should correspond to superoxide ion (O_2^-), which comes from the adsorption of atmospheric oxygen accommodated in surface oxygen vacancies.[44,45] The other three peaks (531.1, 529.8, and 529.0 eV) can be assigned to bridge OH groups, lattice oxygen, and oxygen atoms located near reduced lattice indium and titanium ($R_{(In,Ti)}$), respectively.[44,46−48] Obviously, for ITON350 and ITON500, the peak at around 532.7 eV is absent, indicating no oxygen vacancies in these two samples. In addition, from the N 1s and Ti 2p XPS spectra, doped N and Ti^{3+} are also not present in ITON350 and ITON500.

Electron paramagnetic resonance (EPR) was performed to determine the chemical environment of unpaired electrons, thus further demonstrating the existence of $Ti^{3+}$and oxygen vacancies (Figure 4). EPR signals at g = 1.997 (324.32 MT) and

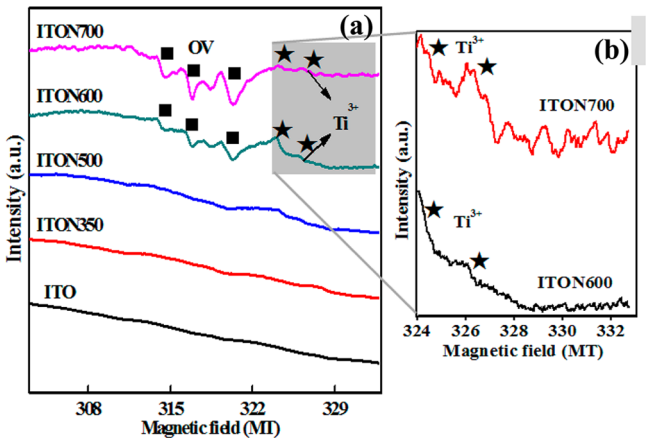

Figure 4. (a) EPR spectra of In_2TiO_5 samples. (b) Partial enlarged EPR spectra of ITON600 and ITON700.

g = 1.981 (326.92 MT) are characteristic of electrons trapped in distorted four-coordinated Ti^{4+} sites, confirming the presence of Ti^{3+} as well as oxygen deficiencies in ITON600 and ITON700.[45,49] The g values at 2.025 (319.81 MT), 2.046 (316.56 MT), and 2.061 (314.18 MT) are in agreement with values reported for oxygen radical species on the catalyst surface.[50,51] According to the literature, the oxygen vacancies are probably induced by doped nitrogen and hydrogen thermal treatment at 600−700 °C by annealing ITO in NH_3 flow. As mentioned above, hydrogen gas can be generated by thermal decomposition of NH_3 at temperatures higher than 600 °C.[52,53] Compared with ITON700, ITON600 exhibits a weak OV signal. Moreover, no evident Ti^{3+} and OV signals are observed in ITON500 and ITON350 or in pristine ITO.

UV−vis−NIR absorption spectra of pristine In_2TiO_5 and NH_3-treated samples are shown in Figure 5a. The evident

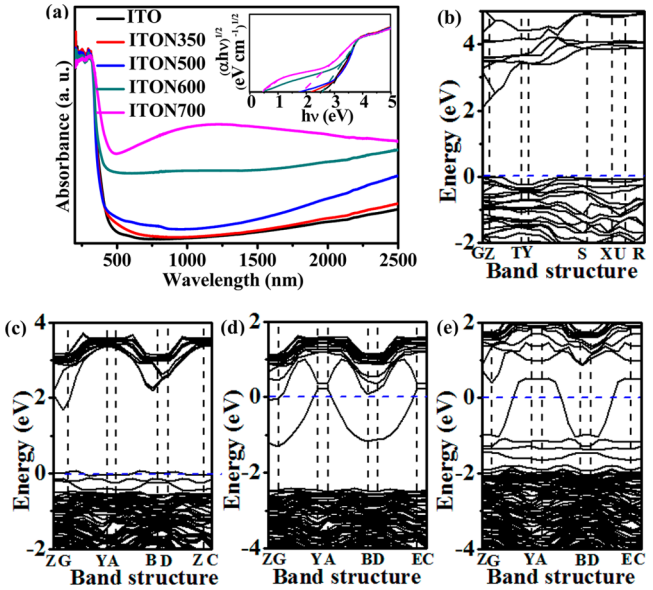

Figure 5. (a) UV−vis−NIR absorption spectra of In_2TiO_5 samples; (inset) Kubelka−Munk transformation of absorption curves. (b−e) Calculated electronic band structures of (b) pristine In_2TiO_5, (c) N-In_2TiO_5, (d) OV-In_2TiO_5, and (e) OV,N-In_2TiO_5.

absorption for all samples at wavelengths shorter than 400 nm can be assigned to the intrinsic band gap absorption of In_2TiO_5. The absorption edges for ITON600 and ITON700 were red-shifted compared to those of other samples, thereby confirming the effectiveness of band gap narrowing by OV and nitrogen doping. It is worth mentioning that ITON600 and ITON700 absorb light in the whole UV−vis−NIR light region (200−2500 nm). The band gap (E_g) can be estimated from the Kubelka−Munk function versus the energy of the light absorbed (inset in Figure 5a). Clearly, ITON350 and ITON500 have almost same E_g as pristine In_2TiO_5 (E_g = 2.83 eV), whereas the band gaps of ITON600 and ITON700 decrease to 2.58 and 1.82 eV, respectively. Moreover, a new band gap (0.45 eV) is observed in ITON700, which comes from the excitation of electrons in the impurity energy levels to the conduction band (CB) by absorbing NIR light.

In the present work, to further understand the origin of the NIR light response and narrowed band gaps of ITON600 and ITON700, calculations based on the DFT method by use of Materials Studio were carried out to determine the electronic band structure of pristine, N-, OV-, and OV,N-In_2TiO_5 (Figure 5b−e). The calculated E_g = 2.1 eV for pristine In_2TiO_5 is not in good agreement with the experimental value of 2.83 eV, which can be ascribed to the nature of the LDA method and the band structure of In_2TiO_5 (Figure 5b).[54] Compared with that of pristine In_2TiO_5, the band gap of N-In_2TiO_5 between the

DOI: 10.1021/acsami.5b05706
ACS Appl. Mater. Interfaces 2015, 7, 20761−20768

unoccupied level and the bottom of the conduction band is about 0.43 eV narrower (Figure 5c), which mainly results from the contribution of hybridization of N 2p with O 2p orbitals, thus leading to the shift of the valence band edge upward.[55,56] However, for OV-In_2TiO_5, a newly formed oxygen vacancy state is observed and is located below the conduction band minimum (CBM), which can serve as the springboard for the photoexcited electrons to jump from the valence band (VB) into gap states and subsequently to the CB under NIR light irradiation (Figure 5d).[12,45] For OV,N-In_2TiO_5, the VB moves upward and impure energy levels are seen in the band gap due to coaction of oxygen vacancies and doped nitrogen, and thus the band gap is reduced to 1.12 eV (Figure 5e). This result is in agreement with that from UV−vis−NIR absorption spectra described above. The narrowed E_g and the new springboard of OV,N-In_2TiO_5 indicate that the oxygen vacancy and nitrogen codoped system may have better NIR light photocatalytic activity than those undoped and monodoped systems.

Figure 6 shows the photocurrent responses of ITO samples to on−off cycling recorded at +1.0 V bias. It can be clearly seen

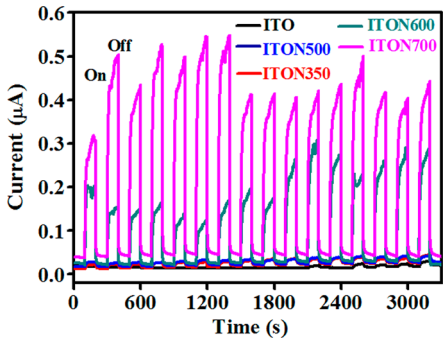

Figure 6. Time-based transient photocurrent responses of In_2TiO_5 samples under NIR light irradiation (760−1100 nm) in aqueous sodium sulfate solution (1 mol·L^{-1}) as supporting electrolyte.

that ITO, ITON350, and ITON500 generated negligible photocurrent, indicating that almost no electrons flow through the external circuit. The photocurrent value increased with increasing NH_3 treatment temperature, and ITON700 showed the highest photocurrent. For ITON700 working electrode, prompt photocurrent generation was observed once NIR light was turned on and the photocurrent value decreased to near zero as soon as the light was turned off. Although a relatively large photocurrent fluctuation was observed before 1500 s, the photocurrent could keep stable after 1500 s. Therefore, it can be concluded that during the 16 on−off irradiation cycles, the generated photocurrents can be considered comparatively stable. The prompt photocurrent response of ITON700 indicates its highly efficient separation and transfer of the charge under NIR light irradiation.[57]

In view of the NIR photocurrent responses, we further studied the NIR light-driven photocatalytic H_2 production of In_2TiO_5 samples. The photocatalytic reaction setup, optical spectrum analyzer, and emission spectra of Xe lamp used in our experiments are presented in Figures S2−S4. It can be seen that the NIR light we used was 760−1100 nm (Figure S4). Figure 7 panels a−e show GC traces of the headspace over 9 h of photocatalytic reaction of Pt-loaded In_2TiO_5 samples in pure H_2O under NIR light. Obviously, no photocatalytic activity toward H_2 production was observed on ITO, ITON350, and ITON500 under NIR light irradiation, and ITON600 showed poor activity with 0.53 μmol of H_2 produced after 9 h (Figure 7a−d). The H_2 signals produced by ITON700 as a function of NIR light irradiation time are presented in Figure 7e, which shows that the H_2 evolution rate steadily increases during a long photocatalytic reaction and the total amount of H_2 is 11.2 μmol after 9 h. If the ITON700 sample was put in the dark, no H_2 was evolved, confirming the fact that the reaction is driven by NIR light and no thermocatalytic H_2 was evolved under the present conditions. For comparison, we also performed the experiment of single Pt in pure H_2O under NIR light irradiation, and no H_2 was generated. These results clearly demonstrate the NIR light photocatalytic H_2 production ability of ITON700 photocatalyst with Pt as a cocatalyst. From these photocatalytic experimental results, we deduce that the ITO samples annealed in low NH_3 treatment temperatures lack OV and N-doping, and therefore the valence electrons cannot be excited by NIR light, while those samples obtained at NH_3 treatment temperatures higher than 600 °C contain OV and N-doping, and thus the band structure was changed toward NIR light-responsive. Therefore, OV and N-doping are crucial for efficient NIR light photocatalytic H_2 production due to the fact

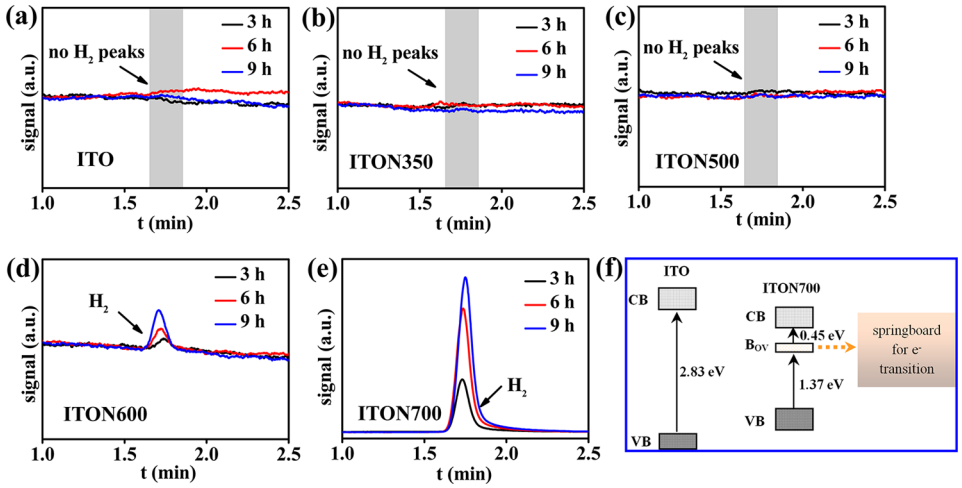

Figure 7. (a−e) GC traces of the headspace over 9 h of photocatalytic reaction of Pt-loaded In_2TiO_5 samples in pure H_2O under NIR light. (f) Schematic band structures of ITO and ITON700.

DOI: 10.1021/acsami.5b05706
ACS Appl. Mater. Interfaces 2015, 7, 20761−20768

that an interband springboard in ITON700 is indispensable for the excitation of photoelectrons from VB to CB under NIR light irradiation (Figure 7f). Obviously, the enhanced NIR absorption of ITON700 will be beneficial for harvesting a wide range of light.

Moreover, In_2TiO_5 samples obtained at NH_3 treatment temperatures higher than 700 °C (denoted as ITON750, ITON800, and ITON900) were also tested for NIR light photocatalytic H_2 production. As the heat-treatment temperature increased from 700 to 900 °C, the H_2 production rate decreased. There is a sharp decrease in the photocatalytic H_2 production rate from 1.36 μmol in 9 h for ITON750 to 0 μmol of H_2 for both ITON800 and ITON900 (Figure S6a–c). This is because when the NH_3 treatment temperature was higher than 800 °C, no In_2TiO_5 phase was formed and the as-obtained samples (ITON800 and ITON900) were mainly a mixture of In and TiN (Figure S5a). Electronic band structure calculation of TiN clearly indicates a metallic structure, with the Fermi level located within the CB and intersecting several bands (Figure S7).[58] For ITON750, we know that a small amount of In_2TiO_5 has been reduced to In (Figure S5a), which may be the main reason for a sharp decrease in the photocatalytic H_2 production rate compared to ITON700. In view of the metallic properties of In and TiN, and their inefficient performance in NIR photocatalysis with ITON800 and ITON900, the excellent photocatalysis performance for H_2 production with ITON750 can be ascribed to its VO and N-doping.

To further analyze the NIR light-driven photocatalytic performance of OV-In_2TiO_5 samples without N-doping, pristine In_2TiO_5 was annealed in H_2 flow at 600 and 700 °C to obtain OV-In_2TiO_5 samples, which were denoted as ITOH600 and ITOH700, respectively. The NIR light photocatalytic H_2 production rate was close to zero for both samples (Figure S6d,e). Like ITON600 and ITON700, ITOH600 and ITOH700 were also confirmed to be pure orthorhombic In_2TiO_5 phase (Figure S5b). Moreover, XPS spectra of ITOH700 (Figure S8) indicate that this sample is also rich in Ti^{3+} and oxygen vacancies. As indicated by the theoretical calculations in Figure 5d, there is a defect-related new band occupied with electrons in ITOH700, and thus photoexcitation is allowed from the new band to the CB under NIR light irradiation. The NIR light-driven photoexcitation property of ITOH700 was confirmed by the optical absorption spectra in Figure S9. From the above analysis, we deduce that the possible reason for poorer photocatalytic performance of ITOH600 and ITOH700 may be due to their absence of N-doping, which greatly decreases their optical absorption intensity for NIR light.[45]

In order to optimize the photocatalytic reaction conditions of ITON700, different sacrificial reagents were used, ensuring that the holes were removed quickly from the catalyst, as shown in Figure 8a. The H_2 evolution rates on ITON700 for different sacrificial reagents are in the order methanol > formic acid > ED2Na > ascorbic acid > Na_2S + Na_2SO_3 > triethanolamine, and the highest H_2 evolution rate is 169.8 μmol·g^{-1}·h^{-1}. The H_2 evolution rate is higher than those of reported catalysts focused on wavelengths longer than 760 nm (Table S2). Figure 8b shows a typical time course of H_2 evolution on ITON700 in methanol solution under NIR light irradiation. After illumination for 24 h, although a slight deactivation was observed, the photocatalytic activity remained comparatively stable when the reaction solution was replaced periodically with fresh methanol solution.

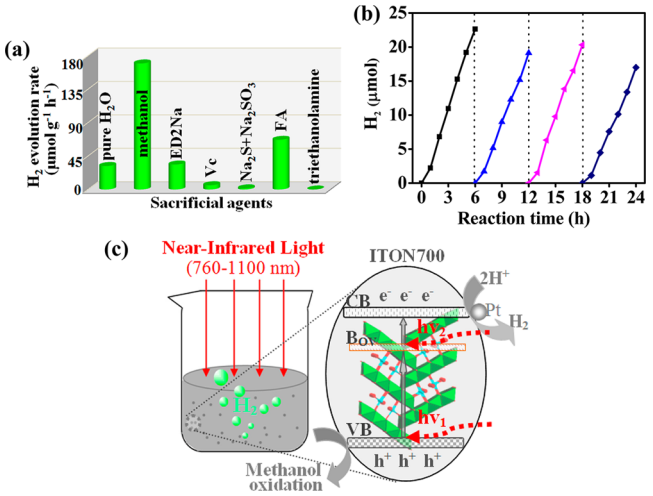

Figure 8. (a) Dependence of H_2 production activity of ITON700 on hole scavengers under NIR light. (b) Time course of photocatalytic H_2 production on ITON700 (30 mg) in methanol solution under NIR light. (c) NIR light photocatalytic reaction model of ITON700 suspended in methanol aqueous solution.

From the above discussion, it can be deduced that, in the H_2O–CH_3OH–ITON700 system under NIR light irradiation, electrons can be excited by NIR light with shorter wavelengths ($h\nu_1 \geq 1.37$ eV; λ_1 = 760–905 nm) from the VB to the interband springboard created by oxygen vacancies below the CB. These electrons can be excited to the CB by NIR light with longer wavelengths ($h\nu_2 \geq 0.45$ eV; λ_2 = 905–1100 nm). Next the electrons transfer to Pt deposited on the surface of ITON700, and eventually they react with the adsorbed H^+ ions to produce H_2. On the other hand, the resulting electron-deficient ITON700 oxidizes CH_3OH and returns to the original state (Figure 8c). In this way, the NIR light energy can be fully used, which may offer new opportunities for sustainable utilization of solar energy in chemistry, especially for photocatalytic H_2 production from water.

4. CONCLUSION

In summary, a novel and robust semiconductor, OV,N-In_2TiO_5, has been synthesized by a multistep sol–gel calcination process and for the first time used for NIR light-driven photocatalytic H_2 production. Under optimal conditions, this photocatalyst is capable of producing H_2 with a rate of 169.8 μmol·(g of catalyst)$^{-1}$·h^{-1} with Pt as cocatalyst, which is very high under NIR irradiation. Theoretical calculations and experimental results demonstrated that it is oxygen vacancies and nitrogen doping that account for the NIR light-responsive abilities by forming an interband springboard and narrowing the band gap. The present work may present a promising future for better design and preparation of photocatalyst, which could result in enhanced NIR light conversion applications and efficiently harvest the wide spectrum of solar light.

■ ASSOCIATED CONTENT

Supporting Information

The Supporting Information is available free of charge on the ACS Publications website at DOI: 10.1021/acsami.5b05706.

XRD patterns of various samples; characterization of ITO samples; reaction setup for photocatalytic H_2 production; photograph of optical spectrum analyzer;

DOI: 10.1021/acsami.5b05706
ACS Appl. Mater. Interfaces 2015, 7, 20761–20768

emission spectra of Xe lamp; GC traces of headspace over 9 h of photocatalytic reaction; calculated electronic band structure of TiN; XPS and UV−vis−NIR spectra of ITOH700 (PDF)

AUTHOR INFORMATION

Corresponding Authors

*(M.C.) Fax +86-10-68912631; tel +86-10-68918468; e-mail caomh@bit.edu.cn.

*(C.H.) Fax +86-10-68912631; tel +86-10-68918468; e-mail cwhu@bit.edu.cn.

Notes

The authors declare no competing financial interest.

ACKNOWLEDGMENTS

This work was supported by the Natural Science Foundation of China (NSFC 21173021, 21231002, 21276026, 21471016, and 21271023), the 973 Program (2014CB932103), and the 111 Project (B07012).

REFERENCES

(1) Esswein, A. J.; Nocera, D. G. Hydrogen Production by Molecular Photocatalysis. *Chem. Rev.* **2007**, *107*, 4022−4047.

(2) Murdoch, M.; Waterhouse, G. I. N.; Nadeem, M. A.; Metson, J. B.; Keane, M. A.; Howe, R. F.; Llorca, J.; Idriss, H. The Effect of Gold Loading and Particle Size on Photocatalytic Hydrogen Production from Ethanol over Au/TiO_2 Nanoparticles. *Nat. Chem.* **2011**, *3*, 489−492.

(3) Ha, E.; Lee, L. Y.; Wang, J.; Li, F.; Wong, K. Y.; Tsang, S. C. Significant Enhancement in Photocatalytic Reduction of Water to Hydrogen by Au/Cu_2ZnSnS_4 Nanostructure. *Adv. Mater.* **2014**, *26*, 3496−3500.

(4) Xie, Y.; Yu, Z.; Liu, G.; Ma, X.; Cheng, H. CdS-Mesoporous ZnS Core-Shell Particles for Efficient and Stable Photocatalytic Hydrogen Evolution under Visible Light. *Energy Environ. Sci.* **2014**, *7*, 1895−1901.

(5) Liu, S.; Yu, J.; Jaroniec, M. Tunable Photocatalytic Selectivity of Hollow TiO_2 Microspheres Composed of Anatase Polyhedra with Exposed {001} Facets. *J. Am. Chem. Soc.* **2010**, *132*, 11914−11916.

(6) Zou, Z.; Ye, J.; Sayama, K.; Arakawa, H. Direct Splitting of Water under Visible Light Irradiation with an Oxide Semiconductor Photocatalyst. *Nature* **2001**, *414*, 625−627.

(7) Zuo, F.; Bozhilov, K.; Dillon, R. J.; Wang, L.; Smith, P.; Zhao, X.; Bardeen, C.; Feng, P. Active Facets on Titanium(III)-Doped TiO_2: An Effective Strategy toImprove the Visible-Light Photocatalytic Activity. *Angew. Chem., Int. Ed.* **2012**, *51*, 6223−6226.

(8) Pang, H.; Wei, C.; Li, X.; Li, G.; Ma, Y.; Li, S.; Chen, J.; Zhang, J. Microwave-Assisted Synthesis of NiS_2 Nanostructures for Supercapacitors and Cocatalytic Enhancing Photocatalytic H_2 Production. *Sci. Rep.* **2014**, *4*, 3577.

(9) Wu, X.; Yin, S.; Dong, Q.; Sato, T. Blue/green/red Colour Emitting Up-conversion Phosphors Coupled C-TiO_2 Composites with UV, Visible and NIR Responsive Photocatalytic Performance. *Appl. Catal., B* **2014**, *156-157*, 257−264.

(10) Li, C.; Wang, F.; Zhu, J.; Yu, J. C. $NaYF_4$:Yb,Tm/CdS Composite as a Novel Near-Infrared-Driven Photocatalyst. *Appl. Catal., B* **2010**, *100*, 433−439.

(11) Wang, G.; Huang, B.; Ma, X.; Wang, Z.; Qin, X.; Zhang, X.; Dai, Y.; Whangbo, M. H. $Cu_2(OH)PO_4$, a Near-Infrared-Activated Photocatalyst. *Angew. Chem., Int. Ed.* **2013**, *52*, 4810−4813.

(12) Tian, J.; Sang, Y.; Yu, G.; Jiang, H.; Mu, X.; Liu, H. A Bi_2WO_6-Based Hybrid Photocatalyst with Broad Spectrum Photocatalytic Properties under UV, Visible, and Near-Infrared Irradiation. *Adv. Mater.* **2013**, *25*, 5075−5080.

(13) Chen, X.; Liu, L.; Yu, P. Y.; Mao, S. S. Increasing Solar Absorption for Photo- catalysis with Black HydrogenatedTitanium Dioxide Nanocrystals. *Science* **2011**, *331*, 746−750.

(14) Zhang, X.; Peng, T.; Yu, L.; Li, R.; Li, Q.; Li, Z. Visible/Near-Infrared-Light- Induced H_2 Production over g-C_3N_4 Cosensitized by Organic Dye and Zinc Phtha-locyanine Derivative. *ACS Catal.* **2015**, *5*, 504−510.

(15) Li, X.; Li, Z.; Yang, J. Proposed Photosynthesis Method for Producing Hydrogen from Dissociated Water Molecules Using Incident Near-Infrared Light. *Phys. Rev. Lett.* **2014**, *112*, 018301.

(16) Zheng, Z.; Tachikawa, T.; Majima, T. Single-Particle Study of Pt-Modified Au Nanorods for Plasmon-Enhanced Hydrogen Generation in Visible to Near-Infrared Region. *J. Am. Chem. Soc.* **2014**, *136*, 6870−6873.

(17) Zhang, X.; Yu, L.; Zhuang, C.; Peng, T.; Li, R.; Li, X. Highly Asymmetric Phthalocyanine as a Sensitizer of Graphitic Carbon Nitride for Extremely Efficient Photocatalytic H_2 Production under Near-Infrared Light. *ACS Catal.* **2014**, *4*, 162−170.

(18) Pan, L.; Zou, J. J.; Zhang, X.; Wang, L. Water-Mediated Promotion of Dye Sensitization of TiO_2 under Visible Light. *J. Am. Chem. Soc.* **2011**, *133*, 10000−10002.

(19) Choi, W.; Termin, A.; Hoffmann, M. R. The Role of Metal Ion Dopants in Quantum-Sized TiO_2: Correlation between Photoreactivity and Charge Carrier Recombination Dynamics. *J. Phys. Chem.* **1994**, *98*, 13669−13679.

(20) Liu, R.; Hu, P.; Chen, S. Photocatalytic Activity of Ag_3PO_4 Nanoparticle/TiO_2 Nanobelt Heterostructures. *Appl. Surf. Sci.* **2012**, *258*, 9805−9809.

(21) Asahi, R.; Morikawa, T.; Ohwaki, T.; Aoki, K.; Taga, Y. Visible-Light Photocatalysis in Nitrogen-Doped Titanium Oxides. *Science* **2001**, *293*, 269−271.

(22) Burda, C.; Lou, Y.; Chen, X.; Samia, A. C. S.; Stout, J.; Gole, J. L. Enhanced Nitrogen Doping in TiO_2 Nanoparticles. *Nano Lett.* **2003**, *3*, 1049−1051.

(23) Sathish, M.; Viswanathan, B.; Viswanath, R. P.; Gopinath, C. S. Synthesis, Characterization, Electronic Structure, and Photocatalyti-cActivity of Nitrogen-Doped TiO_2 Nanocatalyst. *Chem. Mater.* **2005**, *17*, 6349−6353.

(24) Gundeboina, R.; Veldurthi, N. K.; Velchuri, R.; Guje, R.; Pola, S.; Muga, V.; Nagegownivari R, M. Photocatalytic Performance of Nitrogen-Doped and Cu^{2+} and Ag^{+} Co-Doped Sodium Trititanate. *Int. J. Appl. Ceram. Technol.* **2015**, *12*, 700−710.

(25) Justicia, I.; Ordejón, P.; Canto, G.; Mozos, J. L.; Fraxedas, J.; Battiston, G. A.; Gerbasi, R.; Figueras, A. Designed Self-Doped Titanium Oxide Thin Films for Efficient Visible-Light photocatalysis. *Adv. Mater.* **2002**, *14*, 1399−1402.

(26) Wang, J.; Wang, Z.; Huang, B.; Ma, Y.; Liu, Y.; Qin, X.; Zhang, X.; Dai, Y. Oxygen Vacancy Induced Band-Gap Narrowing and Enhanced Visible Light Photocatalytic Activity of ZnO. *ACS Appl. Mater. Interfaces* **2012**, *4*, 4024−4030.

(27) Lei, F.; Sun, Y.; Liu, K.; Gao, S.; Liang, L.; Pan, B.; Xie, Y. Oxygen Vacancies Confined in Ultrathin Indium Oxide Porous Sheets for Promoted Visible-Light Water Splitting. *J. Am. Chem. Soc.* **2014**, *136*, 6826−6829.

(28) Guan, M.; Xiao, C.; Zhang, J.; Fan, S.; An, R.; Cheng, Q.; Xie, J.; Zhou, M.; Ye, B.; Xie, Y. Vacancy Associates Promoting Solar-Driven Photocatalytic Activity of Ultrathin Bismuth Oxychloride Nanosheets. *J. Am. Chem. Soc.* **2013**, *135*, 10411−10417.

(29) Tsuchiya, T.; Ochi, M.; Higuchi, T.; Terabe, K.; Aono, M. Effect of Ionic Conductivity on Response Speed of $SrTiO_3$-Based All-Solid-State Electric-Double-Layer Transistor. *ACS Appl. Mater. Interfaces* **2015**, *7*, 12254−12260.

(30) Deng, Z.; Dai, Y.; Chen, W.; Pei, X. Synthesis and Characterization of Singlecrystalline $BaTi_2O_5$ Nanowires. *J. Phys. Chem. C* **2010**, *114*, 1748−1751.

(31) Cavalcante, L. S.; Marques, V. S.; Sczancoski, J. C.; Escote, M. T.; Joya, M. R.; Varela, J. A.; Santos, M. R. M. C.; Pizani, P. S.; Longo, E. Synthesis, Structural Refinement and Optical Behavior of $CaTiO_3$

DOI: 10.1021/acsami.5b05706
ACS Appl. Mater. Interfaces 2015, 7, 20761−20768

Powders: a Comparative Study of Processing in Different Furnaces. *Chem. Eng. J.* **2008**, *143*, 299−307.
(32) Tang, J.; Zou, Z.; Ye, J. Effects of Substituting Sr^{2+} and Ba^{2+} for Ca^{2+} on the Structural Properties and Photocatalytic Behaviors of $CaIn_2O_4$. *Chem. Mater.* **2004**, *16*, 1644−1649.
(33) Wang, W. D.; Huang, F. Q.; Liu, C. M.; Lin, X. P.; Shi, J. L. Preparation, Elec- tronic Structure and Photocatalytic Activity of the In_2TiO_5 Photocatalyst. *Mater. Sci. Eng., B* **2007**, *139*, 74−80.
(34) Shah, P.; Bhange, D. S.; Deshpande, A. S.; Kulkarni, M. S.; Gupta, N. M. Doping-Induced Microstructural, Textural and Optical Properties of $In_2Ti_{1-x}V_xO_{5+\delta}$ Semiconductors and Their Role in the Photocatalytic Splitting of Water. *Mater. Chem. Phys.* **2009**, *117*, 399−407.
(35) Liu, Y.; Chen, G.; Zhou, C.; Hu, Y.; Fu, D.; Liu, J.; Wang, Q. Higher Visible Photocatalytic Activities of Nitrogen Doped In_2TiO_5 Sensitized by Carbon Nitride. *J. Hazard. Mater.* **2011**, *190*, 75−80.
(36) Wu, C. H.; Kuo, C. Y.; Lai, C. H.; Chung, W. Y. Decolorization of C. I. Reac- tive Red 2 by a large specific surface area In_2TiO_5: photodegradation and adsorption. *React. Kinet., Mech. Catal.* **2014**, *111*, 383−392.
(37) Diwald, O.; Thompson, T. L.; Zubkov, T.; Walck, S. D.; Yates, J. T. Photo-chemical Activity of Nitrogen-Doped Rutile TiO_2(110) in Visible Light. *J. Phys. Chem. B* **2004**, *108*, 6004−6008.
(38) Gaewdang, T.; Chaminade, J. P.; Gravereau, P.; Garcia, A.; Fouassier, C.; Hagenmuller, P.; Mahiou, R. Crystal Structure and Luminescent Properties of Indium Titanate. *Mater. Res. Bull.* **1993**, *28*, 1051−1060.
(39) Wang, D. H.; Jia, L.; Wu, X. L.; Lu, L. Q.; Xu, A. W. One-Step Hydrothermal Synthesis of N-doped TiO_2/C Nanocomposites with High Visible Light Photocatalytic Activity. *Nanoscale* **2012**, *4*, 576−584.
(40) Xie, J.; Zhang, H.; Li, S.; Wang, R.; Sun, X.; Zhou, M.; Zhou, J.; Lou, X. W.; Xie, Y. Defect-Rich MoS_2 Ultrathin Nanosheets with Additional Active Edge Sites for Enhanced Electrocatalytic Hydrogen Evolution. *Adv. Mater.* **2013**, *25*, 5807−5813.
(41) Graciani, J.; Nambu, A.; Evans, J.; Rodriguez, J. A.; Sanz, J. F. Au ↔N Synergy and N-Doping of Metal Oxide-Based Photocatalysts. *J. Am. Chem. Soc.* **2008**, *130*, 12056−12063.
(42) Gai, L.; Ma, L.; Jiang, H.; Ma, Y.; Tian, Y.; Liu, H. Nitrogen-Doped In_2O_3 Nanocrystals Constituting Hierarchical Structures with Enhanced Gas-Sensing Properties. *CrystEngComm* **2012**, *14*, 7479−7486.
(43) Su, J.; Zou, X. X.; Zou, Y. C.; Li, G. D.; Wang, P. P.; Chen, J. S. Porous Titania with Heavily Self-Doped Ti^{3+} for Specific Sensing of CO at Room Temperature. *Inorg. Chem.* **2013**, *52*, 5924−5930.
(44) Hafeez, M.; Zhai, T.; Bhatti, A. S.; Bando, Y.; Golberg, D. Oxygen Vacancy Driven Modulations in In_2O_3 Pyramidal Beaded Nanowires. *Cryst. Growth Des.* **2012**, *12*, 4935−4943.
(45) Xie, K.; Umezawa, N.; Zhang, N.; Reunchan, P.; Zhang, Y.; Ye, J. Self-Doped $SrTiO_{3-\delta}$ Photocatalyst with Enhanced Activity for Artificial Photosynthesis under Visible Light. *Energy Environ. Sci.* **2011**, *4*, 4211−4219.
(46) Li, J.; Liu, Y.; Zhu, Z.; Zhang, G.; Zou, T.; Zou, Z.; Zhang, S.; Zeng, D.; Xie, C. A Full-Sunlight-Driven Photocatalyst with Super Long-Persistent Energy Storage Ability. *Sci. Rep.* **2013**, *3*, 2409.
(47) Chakraborty, A. K.; Rhaman, M. M.; Hossain, M. E.; Sobahan, K. M. A. Pre- paration of $WO_3/TiO_2/In_2O_3$ Composite Structures and Their Enhanced Photocatalytic Activity under Visible Light Irradiation. *React. Kinet., Mech. Catal.* **2014**, *111*, 371−382.
(48) Li, H.; Schirra, L. K.; Shim, J.; Cheun, H.; Kippelen, B.; Monti, O. L. A.; Bredas, J. L. Zinc Oxideas a Model Transparent Conducting Oxide: A Theoretical and Experimental Study of the Impact of Hydroxylation, Vacancies, Interstitials, and Extrinsic Doping on the Electronic Properties of the Polar ZnO (0002) Surface. *Chem. Mater.* **2012**, *24*, 3044−3055.
(49) Zhang, Z.; Long, J.; Xie, X.; Zhuang, H.; Zhou, Y.; Lin, H.; Yuan, R.; Dai, W.; Ding, Z.; Wang, X.; Fu, X. Controlling the Synergistic Effect of Oxygen Vacancies and N Dopants to Enhance Photocatalytic Activity of N-Doped TiO_2 by H_2 Reduction. *Appl. Catal., A* **2012**, *425−426*, 117−124.
(50) Chen, X.; Wang, X.; Hou, Y.; Huang, J.; Wu, L.; Fu, X. The Effect of Postnitri- dation Annealing on the Surface Property and Photocatalytic Performance of N-Doped TiO_2 under Visible Light Irradiation. *J. Catal.* **2008**, *255*, 59−67.
(51) Strunk, J.; Vining, W. C.; Bell, A. T. A Study of Oxygen Vacancy Formation and Annihilation in Submonolayer Coverages of TiO_2 Dispersed on MCM-48. *J. Phys. Chem. C* **2010**, *114*, 16937−16945.
(52) Di Valentin, C.; Pacchioni, G.; Selloni, A.; Livraghi, S.; Giamello, E. Charac- terization of Paramagnetic Species in N-Doped TiO_2 Powders by EPR Spectroscopy and DFT Calculations. *J. Phys. Chem. B* **2005**, *109*, 11414−11419.
(53) Liu, H.; Ma, H.; Li, X.; Li, W.; Wu, M.; Bao, X. The Enhancement of TiO_2 Photocatalytic Activity by Hydrogen Thermal Treatment. *Chemosphere* **2003**, *50*, 39−46.
(54) Ji, S. M.; Borse, P. H.; Kim, H. G.; Hwang, D. W.; Jang, J. S.; Bae, S. W.; Lee, J. S. Photocatalytic Hydrogen Production from Water-Methanol Mixtures Using N-Doped $Sr_2Nb_2O_7$ under Visible Light Irradiation: Effects of Catalyst Structure. *Phys. Chem. Chem. Phys.* **2005**, *7*, 1315−1321.
(55) Wang, J.; Tafen, D. N.; Lewis, J. P.; Hong, Z.; Manivannan, A.; Zhi, M.; Li, M.; Wu, N. Origin of Photocatalytic Activity of Nitrogen-Doped TiO_2 Nanobelts. *J. Am. Chem. Soc.* **2009**, *131*, 12290−12297.
(56) Wei, W.; Dai, Y.; Guo, M.; Yu, L.; Jin, H.; Han, S.; Huang, B. Codoping Synergistic Effects in N-Doped $SrTiO_3$ for Higher Energy Conversion Efficiency. *Phys. Chem. Chem. Phys.* **2010**, *12*, 7612−7619.
(57) Wang, X.; Wang, J.; Cui, Z.; Wang, S.; Cao, M. Facet Effect of α-Fe_2O_3 Crystals on Photocatalytic Performance in the Photo-Fenton Reaction. *RSC Adv.* **2014**, *4*, 34387−34394.
(58) Yakovkin, I. N. Band Structure of Au Layers on the Ru(0001) and Graphene/Ru(0001) Surfaces. *Eur. Phys. J. B* **2012**, *85*, 61.

DOI: 10.1021/acsami.5b05706
ACS Appl. Mater. Interfaces 2015, 7, 20761−20768